Supporting Information

Harnessing Janus structures: enhanced internal electric fields in C_3N_5 for improved H_2 photocatalysis

Jianwei Yuan[a], Su Li[a], Zhaofei Dang[a], Sixia Liu[b], Fu Yang[c], Dongguang Wang [b], Hengcong Tao*[,b], Shuying Gao*[,b], and Edison Huixiang Ang*[,d]

[a] School of Chemical Engineering and Materials, Changzhou Institute of Technology, 666 Liaohe Road (S), Changzhou, 213022, P. R. China
[b] School of Petrochemical Engineering & Environment, Zhejiang Ocean University, Zhoushan 316022, Zhejiang, P. R. China
[c] School of Environmental and Chemical Engineering, Jiangsu University of Science and Technology, Zhenjiang 212003, Jiangsu, P. R. China
[d] Natural Sciences and Science Education, National Institute of Education, Nanyang Technological University, Singapore 637616, Singapore.

*Corresponding authors; *hengcongtao@zjou.edu.cn* (H. Tao); *gao415127@163.com* (S. Gao); *edison.ang@nie.edu.sg* (E. H. Ang)

S1. Experimental Section

1.1 Photo-electrochemical measurements

The photocurrent, EIS, and Mott-Schottky analyses of Bulk-C_3N_4, Bulk-C_3N_5, and Janus-C_3N_5 were conducted using a CHI660C electrochemical workstation with a standard three-electrode system (Pt foil, Ag/AgCl as reference, and working electrodes) in a 0.5 M Na_2SO_4 solution.

The photocurrent test was performed with an applied potential of 1.1 V (vs Ag/AgCl). For the EIS test, electrochemical impedance spectroscopy (EIS) measurements were taken over a frequency range of 1 Hz to 0.1 MHz. The Mott-Schottky plots, used to calculate the flat band potential, were recorded at frequencies of 500, 1000, and 1500 Hz.

The working electrodes were prepared by dispersing 5 mg of the photocatalyst into 5 mL of ethyl alcohol solution containing 0.5 μL of Nafion and 0.5 μL of distilled water, followed by sonication for an hour. Then, 1 mL of the resulting slurry was spread on a 3 × 1.0 cm FTO glass and allowed to air dry.

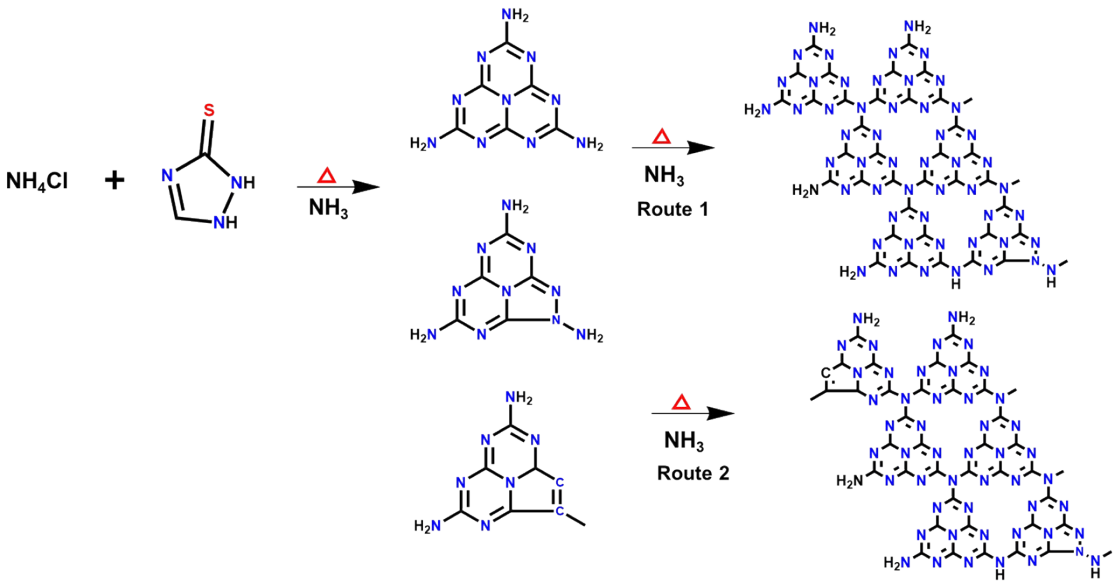

Fig. S1 The proposed reaction pathways for the formation of the Janus-C_3N_5 samples.

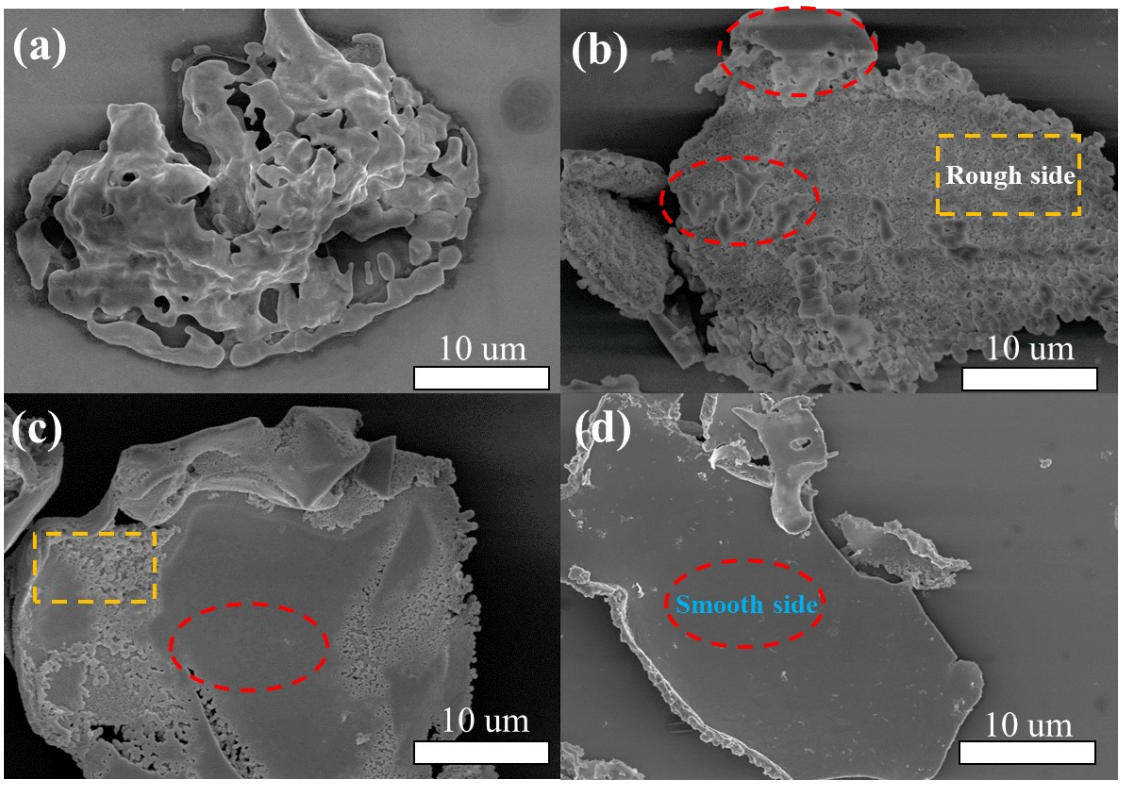

Fig. S2 The SEM images of the (a) Janus-C_3N_5-1h, (b) Janus-C_3N_5-2h, (c) Janus-C_3N_5-3h, and (d) Janus-C_3N_5 samples (4 h).

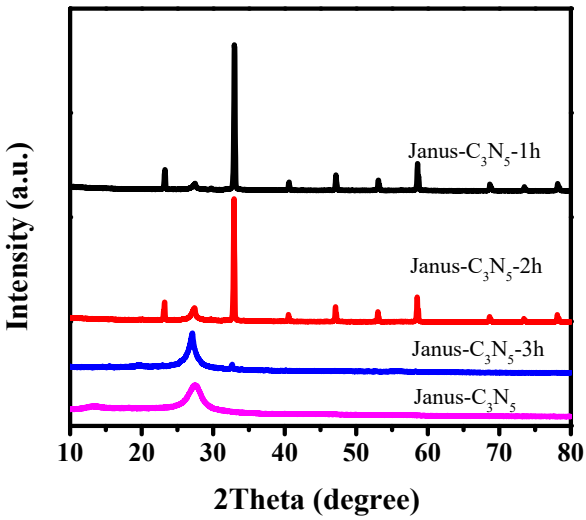

Fig. S3 The XRD patterns of Janus-C_3N_5-1h, Janus-C_3N_5-2h, Janus-C_3N_5-3h, and Janus-C_3N_5 samples (4 h).

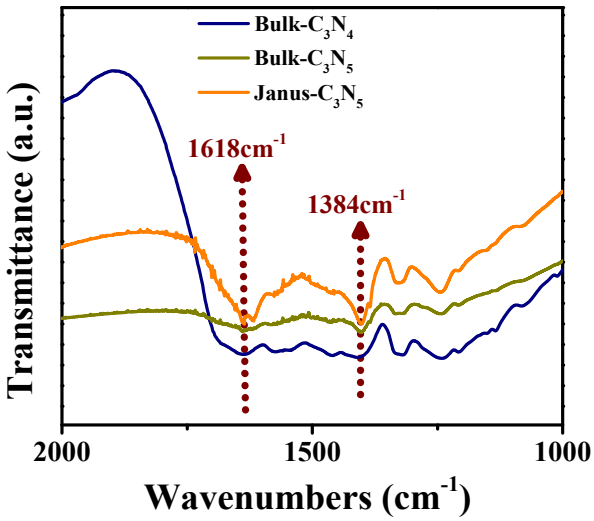

Fig. S4 FT-IR spectra of Bulk-C_3N_4, Bulk-C_3N_5, and Janus-C_3N_5 at (b) 2000 cm^{-1}-100cm^{-1}

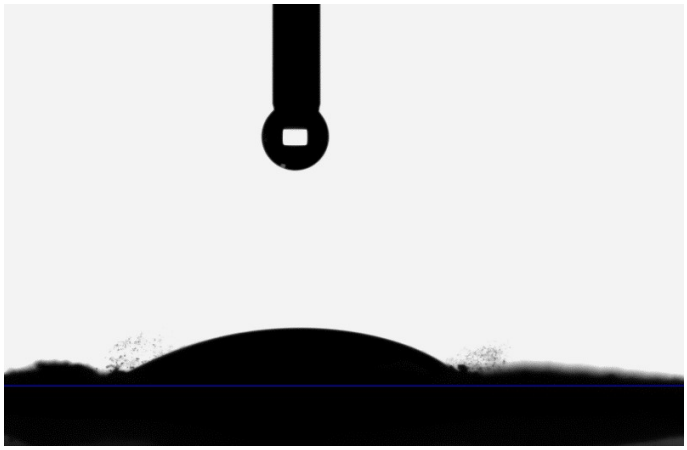

Fig. S5 The static water contact-angle measurement of Bulk-C_3N_4.

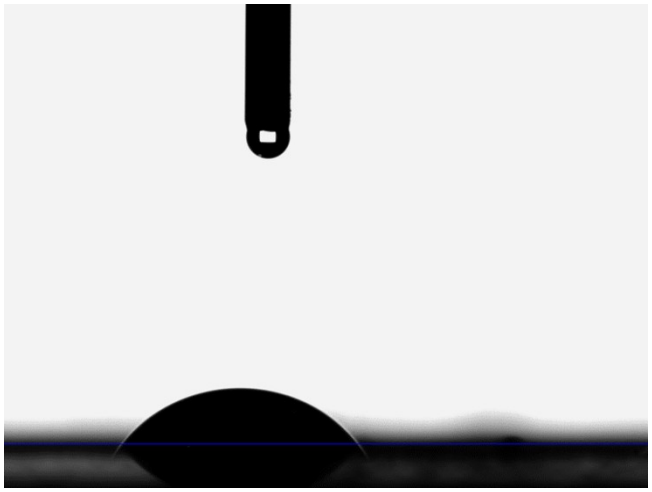

Fig. S6 The static water contact-angle measurement of Bulk-C_3N_5.

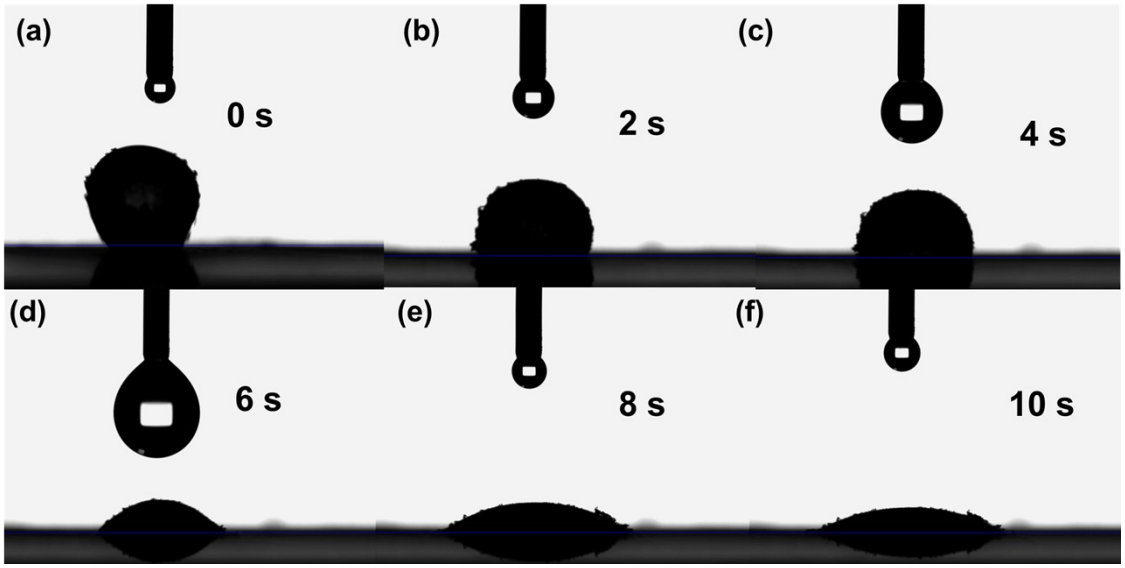

Fig. S7 (a-f) The static water contact-angle measurements of Janus-C_3N_5.

As illustrated in **Fig. S6**, Bulk-C_3N_5 maintains a stable static water contact angle over 10 s. In contrast, the static water contact angle of Janus-C_3N_5 decreases progressively over the same period (**Fig. S7**). Initially, the contact angle is large, with some distortion observed on the surface of the water drop. This phenomenon is likely due to changes in surface tension caused by the different chemical structures, particularly the ultrathin nanosheets of carbon-rich C_3N_5. The contact angle then decreases rapidly within 10 s, which can be attributed to water diffusing into the nitrogen-rich honeycomb network of C_3N_5. Therefore, the variation in static water contact angle over time further confirms the Janus structure of C_3N_5.

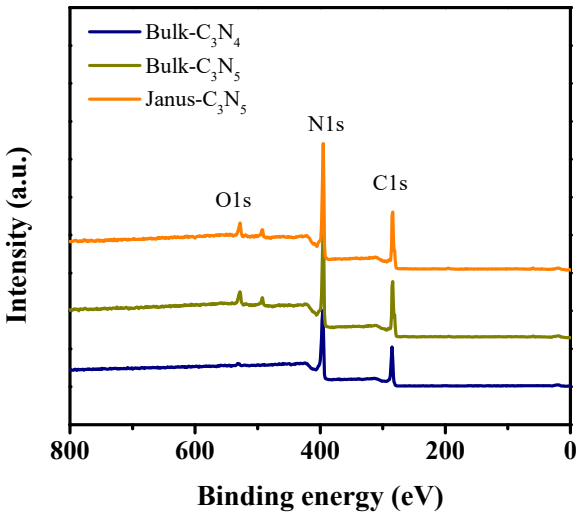

Fig. S8 The survey XPS spectra of Bulk-C_3N_4, Bulk-C_3N_5, and Janus-C_3N_5.

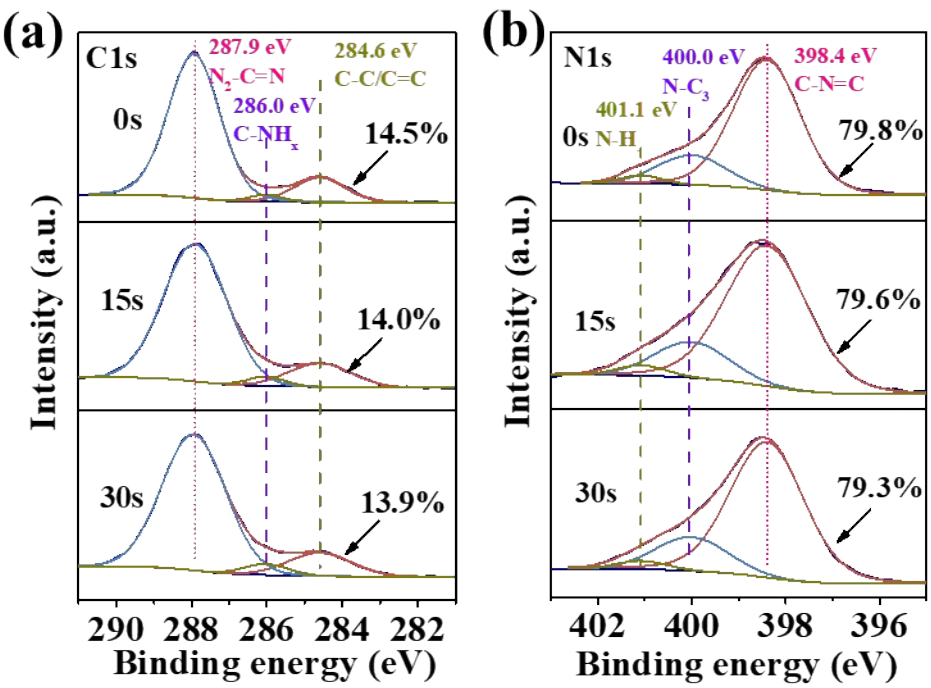

Fig. S9 (a) The C 1s core level XPS spectra and (b) the N 1s core level XPS spectra of Bulk-C_3N_5 samples at different etching times.

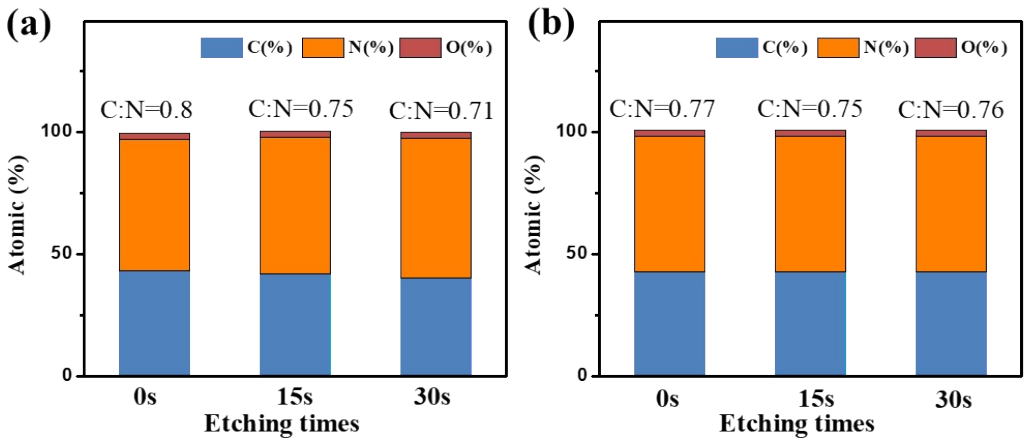

Fig. S10 The surface C and N composition of different samples with with the Ar ion etching process (0s, 15s and 30s) for samples (a) Janus-C_3N_5 and (b) Bulk-C_3N_5 samples.

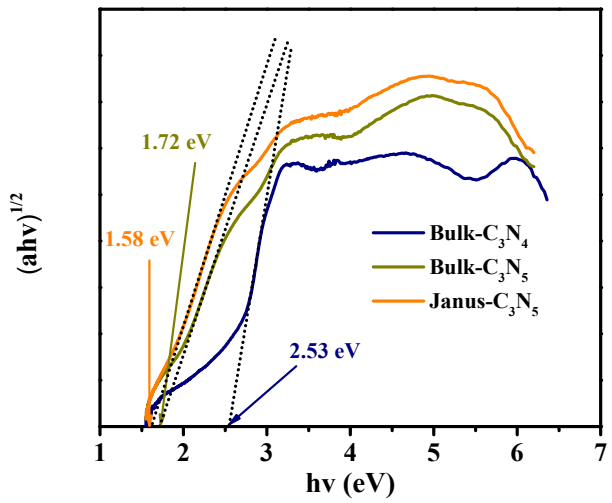

Fig. S11 The band gap energies of Bulk-C_3N_4, Bulk-C_3N_5 and Janus-C_3N_5 samples.

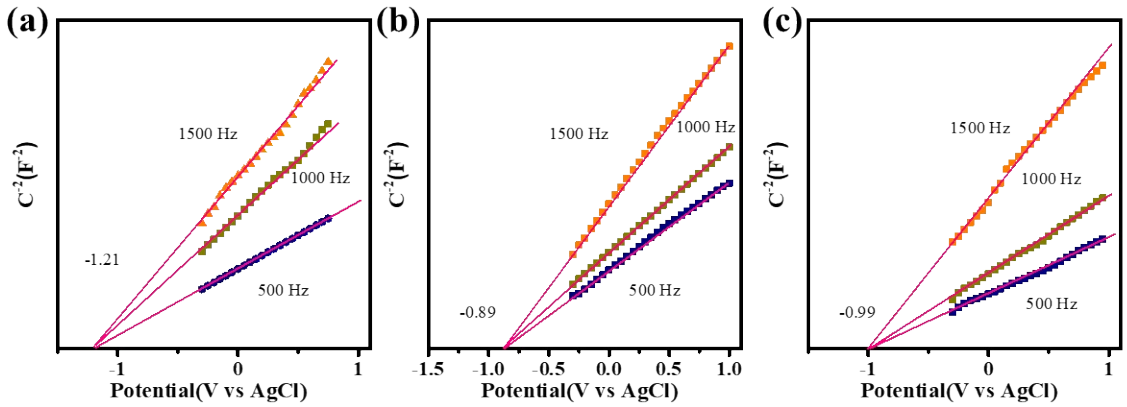

Fig. S12 The Mott-shottky curves of Bulk-C_3N_4, Bulk-C_3N_5 and Janus-C_3N_5 samples.

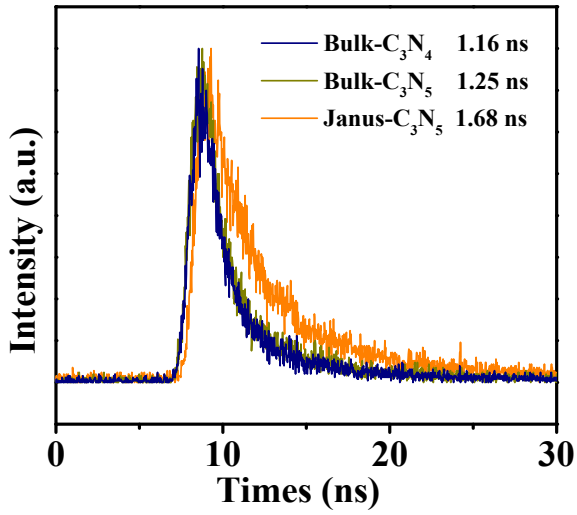

Fig. S13 Photocurrent responses and time-resolved PL decay spectra of Bulk-C_3N_4, Bulk-C_3N_5, and Janus-C_3N_5 samples.

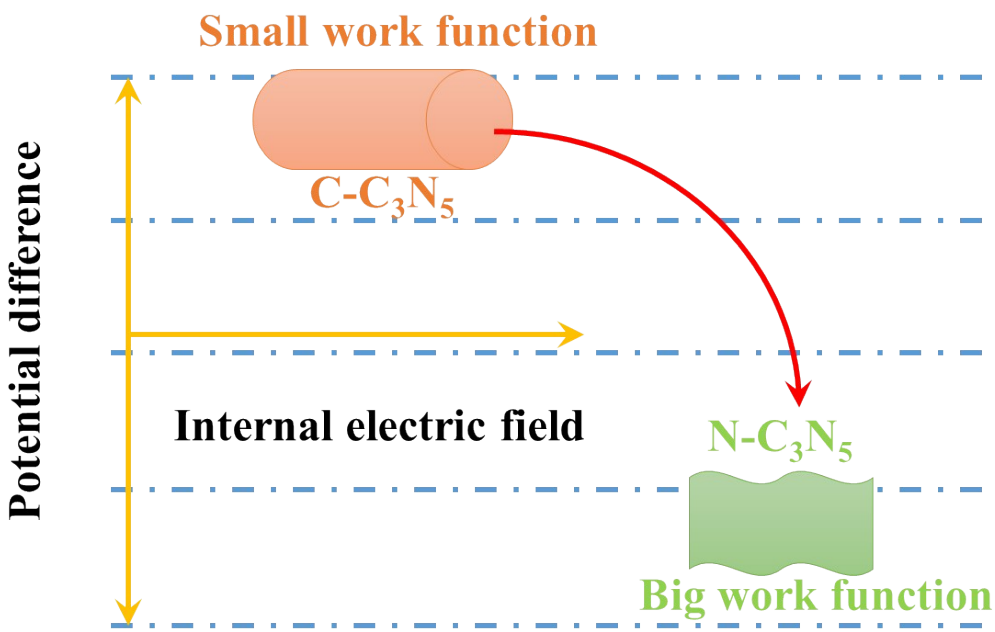

Fig. S14 Schematic illustration of charge transport driven by potential difference.

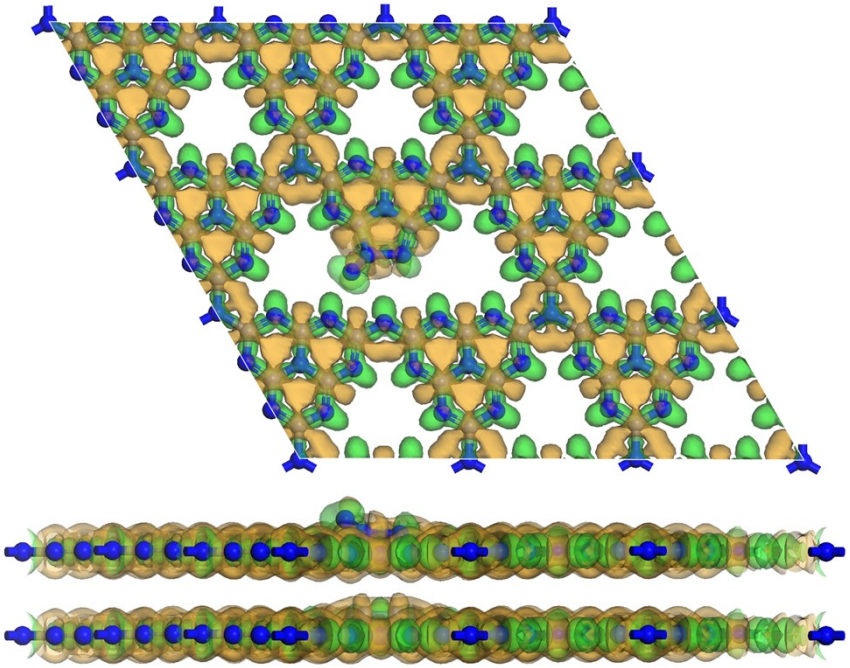

Fig. S15 Charge density difference of CN-C_3N_5 (yellow and blue represent the charge accumulation and loss, respectively).

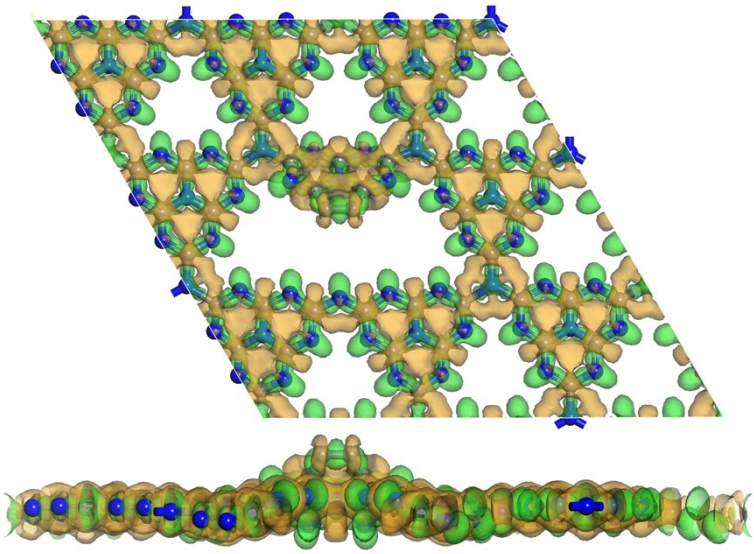

Fig. S16 Charge density difference of C-C_3N_5 (yellow and blue represent the charge accumulation and loss, respectively).

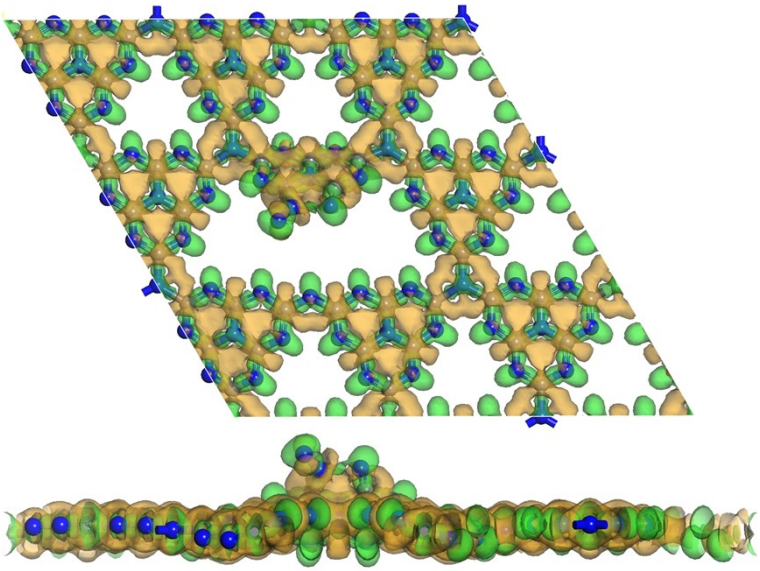

Fig. S17 Charge density difference of N-C_3N_5 (yellow and blue represent the charge accumulation and loss, respectively).